

Vision-Based Power Line Cables and Pylons Detection for Low Flying Aircrafts

Jakub Gwizdała¹, Doruk Oner¹, Soumava Kumar Roy, Mian Akbar Shah, Ad Eberhard², Ivan Egorov², Philipp Krüsi², Grigory Yakushev², Pascal Fua^{1*}

^{1*}Computer Vision Laboratory, EPFL, Switzerland.

²Daedalean AG, Zürich, Switzerland.

*Corresponding author(s). E-mail(s): pascal.fua@epfl.ch;

Contributing authors: jakub.gwizdala@epfl.ch; doruk.oner@epfl.ch; gy@daedalean.ai;

Abstract

Power lines are dangerous for low-flying aircrafts, especially in low-visibility conditions. Thus, a vision-based system able to analyze the aircraft’s surroundings and to provide the pilots with a “second pair of eyes” can contribute to enhancing their safety. To this end, we have developed a deep learning approach to jointly detect power line cables and pylons from images captured at distances of several hundred meters by aircraft-mounted cameras. In doing so, we have combined a modern convolutional architecture with transfer learning and a loss function adapted to curvilinear structure delineation. We use a single network for both detection tasks and demonstrated its performance on two benchmarking datasets. We have integrated it within an onboard system and run it in flight, and have demonstrated with our experiments that it outperforms the prior distant cable detection method [1] on both datasets, while also successfully detecting pylons, given their annotations are available for the data.

Keywords: Power lines detection, Transmission towers detection, Poles detection, Delineation, Deep learning

1 Introduction

Low-flying aircrafts, such as light planes and helicopters, are always at risk of colliding with ground obstacles. Power lines are especially dangerous because they are hard to see, even in good weather. In 2010, the Federal Aviation Administration used 13 years worth of accident data from the National Transportation Safety Board (NTSB) database to estimate that there are 76 collisions with power line per year on average and that 30% of them resulted in fatalities [2]. Utility poles and transmission towers, which we will collectively refer to as *pylons*, constitute additional dangers and are often found in the vicinity of

power line cables. Many of the accidents stem from the fact that pilots are expected to simultaneously carry out many tasks—steering the aircraft, navigating, monitoring the weather, and performing mission-related tasks—that all require a high level of concentration. This sometimes causes cognitive overload and loss of situational awareness [3]. An automated system that would alert the pilots to an impending collision danger would therefore be extremely valuable.

Systems, such as the FLARM [4], which relies on a database of known obstacles, are a good start. However, there always is the possibility of obstacles not being in the database. Thus, there has long been interest in developing video-based

algorithms to detect power line cables. Most early work relied on image processing methods designed for line detection, both for detection of cables [5–8] and pylons [9]. Feature-based machine learning techniques then started being used [6, 10, 11] but were superseded by deep-learning based methods, both for power line cables [12–16] and transmission towers [17]. Most of prior research focuses on either the detection of power line cables or that of pylons [18] and does not treat them jointly. Methods for power line cables detection are frequently developed in the context of power line infrastructure inspection, where the cables are likely to be more clearly visible than at larger distances encountered during regular small aircraft flights. In this work we tackle this latter challenging scenario with the aim of developing an aircraft safety system assisting the pilots in detecting these notorious dangers.

We propose a new deep-learning based approach to jointly detect power line cables and pylons. We use a pre-trained ConvNeXt [19] as our backbone and formulate the detection task as one of regressing a map of distances to the obstacles from the images. To validate our method we compare with approach proposed by Stambler et al. [1] and use the accompanying NE-VBW dataset – a public high-resolution dataset created for vision-based power line cables detection in the context of developing aircraft safety system. We demonstrate that combining transfer learning, a modern backbone, and a suitable loss function designed for curvilinear structure detection boosts performance beyond the previously proposed method [1] on their dataset.

There are other datasets that could be used to evaluate cable detection algorithms [8, 20–26]. However, they have various limitations, including: a viewing perspective from the level close to the ground and mostly in urban settings [8, 26], scaled down higher resolution images with only image-level labels [20, 21], small dataset size [25] or well visible power lines [22, 23], including scenarios intended for testing cable inspection methods with power lines seen from a short distance [24]. We are facing a very different scenario with broad fields of view, distant barely visible power lines and high-resolution images. To develop our detection method we created our more diverse DDLN dataset, recorded with short focals that provide information about a large area in front of the

aircraft. We also evaluate our approach on it and demonstrate the strong performance of our approach. Finally, we show that, given additional annotations for pylons, a single network can easily and successfully be trained to detect them in addition to cables. Furthermore, when only pylon detection is needed and small detection errors are tolerated, it performs competitively to the state-of-the-art real-time object detector [27] of similar size.

In the following section 2 we present prior works on vision-based power line cables and pylons detection. In section 3 we describe our model architecture and the loss function. Section 4 presents our results, accompanied by the descriptions of the datasets used for the evaluation, baselines we compare with and the implementation details. Finally, we summarize our work and discuss the limitations of the presented method together with the possible future directions in section 5.

2 Related works

2.1 Detecting Power Lines

Vision-based detection of power line cables has a long history. Many approaches, including some relatively recent ones, rely on image processing techniques, such as edge detection or the Hough and Radon transforms [5–8, 28–34].

Such detection methods that rely on manually designed image processing pipelines have now been outperformed across the whole computer vision field by learning-based methods, provided that sufficient amount of training data is available. Thus, the approach to cable detection has changed with the advent of deep learning techniques. Several works formulated the detection task as one of classifying image patches according to the presence or absence of power line cables. In [12], previously extracted image edge maps are used as the input to the trained model. In [13], Histogram of Gradient (HoG) features are used instead. The algorithm of [14] performs patch classification and recovers pixel-wise segmentation indirectly by processing intermediate network activations. That of [15] follows a hybrid approach with a hierarchical CNN classifier over a set of different resolution of patches, followed by traditional techniques based on edge filters

and a Hough Transform variant to precisely localize wires. These classification approaches were by design weakly-supervised [14] for cables presence and could not benefit from a richer information about detected objects’ appearance, which can be provided by binary masks and exploited by segmentation-based approaches.

Another line of research focused on using object, line or key points detectors. Nguyen et al. [35] proposed LS-Net, a single-shot detector, combining classification and line endpoints regression tasks, performed over a set of four overlapping grids of cells. Their method has been evaluated on a dataset [22] featuring 800 crops extracted from full HD frames, scaled to 512×512 px patches, with power line cables clearly visible over the terrain background. Abdelfattah et al. [24] introduced the TTPLA dataset, featuring high-resolution aerial images captured by a drone flying within a close distance from power line infrastructure and annotated with cable and transmission tower masks. They also established an instance segmentation baseline with the use of YOLACT [36], an extension of single-shot object detector with a segmentation capability. Recently, Xing et al. [37] designed a power line detection method for use by inspection drones. They used YOLO [38], trained solely on synthetic data which additionally classified the inclination of a power line cable within the detected bounding box. However, as in [24], their data was restricted to close views of power line cables from the perspective of a drone hovering above the inspected infrastructure. Finally, a key point detection scheme was proposed by Dai et al. [39]. They formulate the detection as a regression of 5 key points evenly distributed across each cable in the input image. The points regressed by the network are subsequently clustered and then a curve representing the complete power line cable can be fitted to their locations. Their method was evaluated on PLDU and PLDM datasets [23], which contain in total 860 images with 540×360 px resolution, each of which with several wires to be detected. These datasets feature again very (PLDU) and relatively (PLDM) close views of cables, often clearly visible against an urban (PLDU) or a mountainous (PLDM) scenery. This makes the cable detection task easier than in our challenging setting of detections at significant distances and over complete high-resolution image.

To leverage the precise supervision signal pixel-wise binary masks can provide, multiple methods formulate power line cable detection as a segmentation task. Madaan et al. [16] applied a CNN directly to the images containing wires and treated detection as a semantic segmentation task. Stambler et al. [1] also performed power line detection relying on segmentation objective, however trained jointly with a regression of parameterized line segment proposals. Both of these methods use custom network architectures, including the use of dilated convolutions and trained from scratch. An alternative approach involves reusing a CNN model pre-trained on a large image datasets and fine-tuning for the cable detection task. This was demonstrated by Zhang et al. [23] with a trimmed VGG16 model [40, 41] pre-trained on the ImageNet dataset [42], but only on the comparatively easy PLDU and PLDM datasets [23]. We follow a similar strategy in our own approach.

Other more recent segmentation approaches to power line cables detection included models based on UNet [43] or UNeXt [44] architectures. Others leverage generative adversarial networks (GANs) trained to highlight power lines in the images [45] or added transformer blocks to CNN feature extractors enabling global attention [46]. Most of these methods [44–46] were evaluated on the TTPLA dataset [24], which features high-resolution close views of cables and pylons, mostly suitable for power line infrastructure inspection. Jaffari et al. [43] evaluated their model on IVRL [22] and PLDU [23], both containing well visible cables crossing the images and the former with low variability of wire appearance. Cheng et al. [44] additionally measured their performance on the VITL dataset [25] which is rather scarce with only 400 crops of higher-resolution images, with a size of 256×256 pixels each. In this work, we evaluated the performance of the models on two datasets – NE-VBW [1] and DDLN dataset collected by us – both of which comprise complete, high-resolution images captured from the flying aircrafts within significant distances from the detected cables and pylons, a setting relevant in the development of a system aiming to improve the aircraft safety.

Cable segmentation models have also been used in the field of computational photography, along with a wire segmentation and in-painting model trained to improve the image aesthetics

by removing cables from the photographs. Chiu et al. [26] have collected the WireSegHR dataset containing 6000 very high-resolution images with pixel-wise annotations of wire locations. Judging by the released test set of 420 images, the dataset contains various kinds of wires and cables, along with other elongated objects, often with challenging appearance and poor visibility in a diverse set of urban sceneries and in cluttered scenes. The images were captured from the ground level as in a typical photography setting. This makes for a different viewing perspective than the one encountered by aircraft. In the images from our DDLN dataset and from the NE-VBW dataset [1], on which we evaluated our method, the wires are mostly seen by the aircraft-mounted camera during flight.

In our approach to localizing power line cables instead of segmentation we use distance mask regression, which is a known choice for curvilinear structures detection [47–49]. As such, our method is closest to the regression of line segment proposals in [1]. However, we use a modern convolutional network architecture [19], leverage transfer learning by starting with a model pre-trained on the ImageNet dataset [42] and extend the regression loss function with a component promoting connectivity in the detections, introduced in our earlier work [50].

2.2 Detecting Pylons

The detection of transmission towers and utility poles has also been the focus of much previous work. Close-range and mid-range detection is usually required in the contexts of inspection [17, 51–53], mapping [54], damage assessment [55, 56] and aircraft safety [57]. In contrast, very long-range detection in satellite or aerial images is mostly performed in top-down views [58–62]. There has been less interest in frontal detection in aerial views at a distance of hundreds of meters, which is the focus of this paper.

Like power lines, pylons can be treated either as thin linear objects or as ones comprised of many line segments, which is especially useful when dealing with the skeletal structure of larger towers. Therefore, similar image processing tools have been used in early pylon detection work. Tilawat et al. [9] used an IIR filter followed by a Hough transform to detect linear segments in the

images. Based on Hough counts in local windows, the probability of pylon presence can be assessed. Similarly, Araar et al. [63] detect line segments in the skeleton of towers using a Line Segment Detector (LSD) [64] and the detections are filtered based on their color characteristics. Other works rely instead on keypoint detectors. Zhang et al. [65] used SIFT [66] key points descriptors and matched them with a set of pylon template features, while Cerón et al. [11] used FAST [67] keypoints and ORB [68] descriptors for training a SVM for the classification of image regions. Sampedro et al. [10] obtained the HoG pylon features and used them to train two multi-layer perceptron (MLP) networks. The former performs binary classification of image regions for pylon detection, while the latter was used for classification of pylon structure types.

As with power lines, newer techniques rely on deep learning methods for pylon detection. Bian et al. [17] designed an unmanned aerial vehicle (UAV) navigation system for power line inspection. It relies on detecting transmission towers, for which they used a customized version of Faster R-CNN [69]. Other works leverage various versions of the YOLO [38] detector [52, 53, 55–57, 61, 70]. Detections from an urban road-level perspective also tend to rely on object detectors – Watanabe [51] used SSD [71] and Zhang et al. [54] used RetinaNet [72].

In our work, we depart from these standard approaches and formulate the task as distance mask regression, as when detecting cables. We compare distance mask based pylon detection performance with that of RT-DETR [27], one of the state-of-the-art real-time object detectors, enhanced with SAHI [73] – inference and fine-tuning strategies for high-resolution images. We show that when distinguishing individual pylons as separate objects is not required and small detection errors are tolerated, our model using similar numbers of learnable network weights delivers a competitive performance, as measured by the metrics evaluating detection outputs.

Transmission towers, thanks to their overall greater size and larger thickness of their components, should be easier to detect than power line cables. Their presence is naturally related to that of power line cables. Several works have leveraged this presence as a useful contextual cue to facilitate the subsequent detection of power lines. A

first subgroup of such techniques relies on hierarchical and algorithmic approaches to infer cable presence given tower detections. Haroun et al. [59] infers power line locations from satellite images by simply connecting pairs of closest detected transmission towers forming a single chain of connections. In a more sophisticated algorithm, after detecting the pylons from the point cloud data, Flanigen [3] used the heights, the distances, and the angles formed by a series of detected towers to infer possible cable connections between the pylons. In another hierarchical manner, Li and Chen [74] used pylon detections to restrict the regions of interest for the subsequent detection of cables. In the absence of pylon detections, either because there are none or because of missed detections, they proposed a second, cable-only detection pipeline. These approaches can be understood as using pylon detection as the way of guessing or restricting the area for cables detection. As observed in Li and Chen [74], such methods have only limited applicability when pylons can be detected first [3, 59]. Otherwise, when the support points of the hanging cable are not visible, there remains a need for handling cable-only detection [74]. In our work, we show that the joint detections of both cables and pylons is feasible using a single deep learning model, without any specific supervision relating both of the detections.

Another group of techniques link cable and pylon detections more tightly. Combined evidence for cables and pylons presence was used by Zhang et al. [65] by formulating a Bayesian framework including terms modeling the spatial correlation between the two object types. This formulation was used to determine whether a line detected by a line detector should be considered as a power line cable or not. The method was further developed in [75]. Its flexibility has been increased by replacing the spatial correlations between pylons and cables by an unconstrained set of auxiliary regions, automatically selected in the vicinity of hypothetical power line detections. The results were evaluated on the BHU dataset [65], which features relatively low resolution images and power line infrastructure seen from ground level. In our work, we tackle a different setting, with power lines infrastructure captured in high-resolution images but further from the camera and seen from the perspective of an aircraft-mounted camera with cables visible

against various backgrounds, mostly originating from the terrain behind them.

Most recently, deep learning methods were tried for joint power line cables and pylon detection [18, 76–78]. Two of these methods [18, 78] are instance segmentation approaches that yield detailed segmentation masks for high resolution inputs. Both of them were evaluated on datasets gathered by UAVs. They comprise close views of the power line infrastructure seen from the top. Zhu et al. [18] evaluated their method additionally on the TTPLA dataset [24], which is mostly suitable for power line inspection related tasks. Feng et al. [76] and Zhencang et al. [77] opted for modified YOLOv3 [79] object detectors. The former used the detection and clustering of auxiliary targets, such as transmission towers, to determine power distribution corridors area and filter out power line detections outside of this zone, a method reminiscent of the algorithmic approaches discussed above [59, 74]. The method was evaluated on a dataset of low-voltage power lines in urban setting, in close, inspection views of the power line infrastructure. Finally, Zhencang et al. [77] added to an object detector’s architecture a *relational suggestion network* with an attention mechanism designed to establish relationships between power lines and pylons. While their dataset features more distant views of power lines than others, the images are captured in relatively low resolution of 640×480 pixels, by an infrared camera and from a low altitude of at most 60 m above ground. These are therefore quite different from the ones we use.

3 Method

To jointly detect *cables*—power and telephone lines—and *pylons*—utility poles and transmission towers—we train a *single* CNN based on a modern backbone. Taking our inspiration from the delineation work of [50], we train it to produce distance maps, one from the detected cables and other from the detected pylons. This effectively turns the detection problem into a regression one in which we treat a zero distance as a detection. Our network can be used for cable- or pylon-only detection by simply removing one of its heads.

For cable detection, we differ from the approach of Stambler et al. [1] by predicting only the undirected distance to the closest wire, as

opposed to distance, direction, and a binary value indicating the presence or absence of a cable. The superior performance of our model, which we demonstrate in the result section, is achieved by combining transfer learning, a modern convolutional backbone, and a loss function that favors cable-like topologies.

3.1 Network Architecture

Fig. 1 depicts the architecture of our model. It comprises two main parts, a pre-trained convolutional feature extractor and two small output heads that regress distances maps from the features.

Feature Encoder. As our backbone, we use ConvNeXt-Tiny [19] pre-trained on the ImageNet [42] dataset. We discard its classification head and only use the feature extractor. We can reduce the original model’s size by adapting the number of blocks B , as defined in [19], in the feature extractor by removing the final ones. In this way, we generated the following variants of our model:

- DDLN-S (small) with $B = (3, 3, 1)$,
- DDLN-M (medium) with $B = (3, 3, 5)$,
- DDLN-L (large) with $B = (3, 3, 9)$,
- DDLN-H (huge) with $B = (3, 3, 9, 1)$.

We do not use the layer normalization and strided convolution following the third stage in the complete ConvNeXt-Tiny model. Therefore our models output a $384 \times (H/16) \times (W/16)$ feature map F , where (H, W) is the resolution of the input image. For DDLN-H the feature map is $768 \times (H/32) \times (W/32)$ and the model requires an additional spatial downsampling level.

Output Heads. They are implemented using pixel-wise regression layers coded as 1×1 convolutions. They are applied directly to the feature map F computed by the feature extractor. Distance predictions are obtained using a clamped-ReLU activation, restricting the outputs to the $[0, 1]$ range. Zero denotes the detected object, either a cable or a pylon depending on the model head. One corresponds to a set maximal distance value d_{\max} that denotes an area sufficiently far away from the objects of interest. In our experiments, we take d_{\max} to be 128 pixels at the original input image resolution.

3.2 Loss Function

Given an image \mathbf{I} , our network outputs two distance maps $\hat{\mathbf{x}}^c$ and $\hat{\mathbf{x}}^p$, one from the cables and the other from the pylons. Let us assume we are given ground-truth versions \mathbf{x}^c and \mathbf{x}^p of these distance maps thresholded at the d_{\max} distance introduced above and linearly scaled to the range $[0, 1]$. Our goal is to train the network so that predictions and ground-truth are as similar as possible to each other, while enforcing good connectivity in the cable reconstruction. To this end, we define a composite loss function that is a weighted sum of a data term and a connectivity term, which we describe below.

Data Loss Term \mathcal{L}_{dat} . The simplest way to write a data loss term would be in terms of the Mean Square Difference (MSD) between $\hat{\mathbf{x}}^c$ and \mathbf{x}^c on one hand, and $\hat{\mathbf{x}}^p$ and \mathbf{x}^p on the other. However, this would not account for the imbalance between the number of pixels that belong to target structures and the much larger one of those that do not. To do so, let us consider the frequency function f^k that associates to each pixel \mathbf{x}_i^k its distance value occurrence frequency in \mathbf{x}^k , where k can be either c for cable or p for pylon. In other words, we write

$$f^k(\mathbf{x}_i^k) = \frac{1}{N} \sum_{1 \leq j \leq N} \mathbb{1}(\mathbf{x}_j^k = \mathbf{x}_i^k), \quad (1)$$

where N is the total number of pixels in \mathbf{x}^k and the \mathbf{x}^k distance masks are discretized to integer values. We use f to write the weighted version of MSD

$$\mathcal{L}_{\text{dat}}(\hat{\mathbf{x}}^k, \mathbf{x}^k) = \sum_{1 \leq i \leq N} w(\mathbf{x}_i^k) \|\hat{\mathbf{x}}_i^k - \mathbf{x}_i^k\|^2, \quad (2)$$

$$w(\mathbf{x}_i^k) = (\log(1 + \epsilon + f^k(\mathbf{x}_i^k)))^{-1},$$

where ϵ , which we set to 0.02, has the purpose of preventing division by values close to 0 and therefore caps the weights at values lower than $(\log(1 + \epsilon))^{-1}$. This scheme gives more weight to the sparse features of interest (cables and pylons) and less to the more extensive background regions, mitigating the imbalance in their occurrence frequency. At the same time, it gives greater weights to areas in the $(0, 1)$ range than to the 0-valued areas at the precise location of the detected

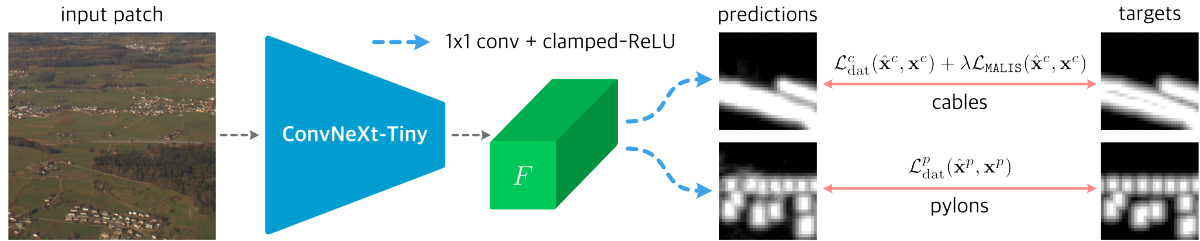


Fig. 1: Architecture of the joint power line cables and pylons detection model. Output heads regress cables and pylons distance masks directly from the common feature map F generated by the fine-tuned truncated ConvNeXt-Tiny feature extractor.

objects. However, thanks to the logarithmic scaling, the difference in weights remains smaller by an order of magnitude than what it would be using inverse frequency weights and avoids excessive penalization of the most frequent distance values – 0 and 1, corresponding to target objects and distant background, respectively.

Connectivity Loss Terms $\mathcal{L}_{\text{MALIS}}$. The loss function \mathcal{L}_{dat} as described above is a pixel-wise loss. When the annotations do not perfectly coincide with the imaged structures, which is often the case, networks trained using such per-pixel losses produce binary masks plagued by topological errors, such as interruptions and missed junctions. In earlier work [50], we introduced a loss function $\mathcal{L}_{\text{MALIS}}$ whose minimization forces to produce distance maps with the same topology as that of the ground truth, even if the actual location of the detection is somewhat imprecise. The difficulty in writing such a loss is to express this requirement in the form of a differentiable loss function that can be used to train a deep network. The central idea of this earlier approach is to forgo enforcing connectivity of the pixels annotated as belonging to linear structures and whose location may be inaccurate. Instead, we express the connectivity of the annotated structures in terms of the disconnections that they create between regions annotated as background. More precisely, we require that two regions separated by a line in the ground truth, are also separated in the prediction. This effectively enforces continuity of the predicted cables. By requiring that connected components of pixels annotated as background remain connected in the prediction, we prevent predicting false positives. To capture dead-ending segments, we compute

our loss in small image windows, which are likely to be subdivided even by short cable sections. In other words, we re-purpose the differentiable machinery proposed in the MALIS segmentation algorithm [80, 81] to enforce the dis-connectivity of image regions separated by cables, which we illustrate in the figure 2. For more details, we refer the interested reader to our earlier publication.

Composite Loss Term \mathcal{L}_{dat} . Given the \mathcal{L}_{dat} and $\mathcal{L}_{\text{MALIS}}$ loss terms defined above, we optimize the composite loss function

$$\mathcal{L}((\hat{\mathbf{x}}^c, \hat{\mathbf{x}}^p), (\mathbf{x}^c, \mathbf{x}^p)) = \mathcal{L}_{\text{dat}}^c(\hat{\mathbf{x}}^c, \mathbf{x}^c) + \mathcal{L}_{\text{dat}}^p(\hat{\mathbf{x}}^p, \mathbf{x}^p) + \lambda \mathcal{L}_{\text{MALIS}}(\hat{\mathbf{x}}^c, \mathbf{x}^c) \quad (3)$$

where upper indices c and p differentiate between cables and pylons and λ is a weighting factor for the MALIS loss component, which we set to 0.2.

4 Results

4.1 Datasets

There are many publicly available annotated datasets that can be used to validate power line detection algorithms. They include USF [8], IVRL [20–22], PLDU and PLDM [23], TTPLA [24], VITL [25] and WireSegHR [26]. As previously discussed in section 1, these have their shortcomings, including: viewing perspective and setting different from the one encountered in manned aircraft flights [8, 26], small size of the dataset with crops of larger images [25], containing scaled down larger images, with low resolution and image-level labels [20, 21] or featuring clearly visible power lines [22–24], oftenly seen from a short

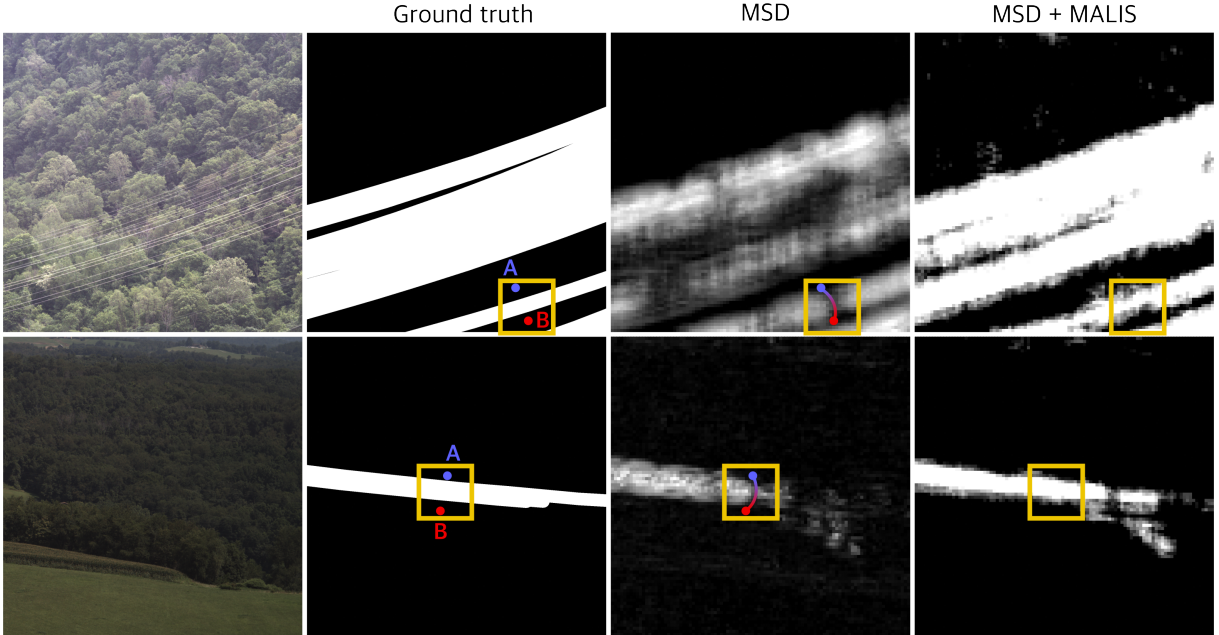


Fig. 2: A selection of two outputs for two loss function variants illustrating the application of $\mathcal{L}_{\text{MALIS}}$ connectivity loss term. The rows contain from left to right: an input image patch, a ground-truth cables segmentation mask, prediction of a model trained with MSD loss alone and prediction of a model trained with MSD loss combined with $\mathcal{L}_{\text{MALIS}}$ connectivity term. The two last images in each row contain distance masks in which $[0, 1]$ values range was mapped to a grayscale range from white to black. $\mathcal{L}_{\text{MALIS}}$ is applied to distance mask predictions within the marked square windows. Points A and B belong to two disjoint background regions, which should be separated by the cable detection in between. In the exemplary distance masks predicted for the cables with independent MSD loss supervision these points can be joined with a path traversing through not sufficiently small distance values. This can result in a broken cable detection in the final segmentation, i.e. in a thresholded distance mask. Such segmentation means having an unwanted merger of the background regions which $\mathcal{L}_{\text{MALIS}}$ aims to prevent.

distance. The latter are more suitable to test algorithms designed to guarantee the safety of UAVs operating in the proximity of the power line infrastructure, mostly for inspection purposes. However, in this work, we want to perform the detection at longer ranges for collision-avoidance purposes. Furthermore, we are doing it in images captured by aircraft-mounted cameras with short focal lengths to cover the large area in front of the aircraft required to ensure safety.

To start developing an aircraft safety system for cable and pylon obstacles avoidance, we created and labeled our own dataset, which we will refer to as the DDLN dataset. The NE-VBW dataset [1] is the publicly available dataset that most resembles ours and was created with the same purpose in mind. We tested our algorithm

on both datasets and we provide additional details below.

NE-VBW Dataset [1]. It is a public dataset containing 109 images of images of size up to 6576×4384 px. They were extracted from recordings captured by aircraft-mounted, forward facing cameras with a large focal length. The high resolution and the large focal length of the cameras allowed for the capture of power line cables at long ranges within a narrow field of view – 25° horizontally and 18° vertically. The images were labeled using pixel-wise masks of power line cables. All data originates from flights conducted around Pittsburgh, PA in the USA.

DDLN Dataset. We built it ourselves from videos acquired during flights over Switzerland, the UK, Brazil, and the USA. It contains 865



Fig. 3: Examples of the images from the NE-VBW dataset [1] (left) and from our DDLN dataset (right).

images of size 4096×3000 px each. They were recorded by aircraft-mounted, forward facing cameras with a wide field of view – up to 81° horizontally and 64° vertically. It is significantly wider than the one in the images from the NE-VBW dataset. This makes the detection task more challenging but provides more context by covering a larger area in front of the aircraft. The videos were recorded at the rate of 6 frames per second, but the annotated frames were extracted with sufficient time intervals between them to provide for a diversified scene content. Polyline approximations of individual power line cables were generated by hand and bounding boxes were used to denote the pylons. Additionally, exclusion areas, that is, regions containing thin objects not associated with cables—flagpoles, cranes, communication towers—were marked by bounding boxes. We did not use them to create training data and excluded them from the pylon detection performance evaluation.

4.2 Baselines

We compare the performance of our models against three baselines: DeepWireCNN [1], PIDNet-S [82] and RT-DETR [27]. We chose the first as the only method which has been so far evaluated for the detection of far-away cables on the NE-VBW dataset. We chose the other two as modern representatives of semantic segmentation and object detection network architectures, respectively, and because they were designed with issues of inference speed in mind. This is an important consideration for the deployment of deep

networks that must run in real-time on hardware that can be installed in an aircraft.

We compare cable detection performance obtained by our models against that of DeepWireCNN on both datasets, while the remaining comparisons are done on the DDLN dataset alone.

We present each of the baselines in more detail below.

DeepWireCNN [1] – cable detection. It is a cable detection model introduced jointly with the NE-VBW dataset. We reimplemented the CNN as described in the publication. However, we did not reimplement the post-processing steps involving clustering of the regressed line segments and a refinement with moving least squares which ultimately led to the generation of segmentation masks at input image resolution. This makes it simple to compare the performance of DeepWireCNN against ours using the coarse resolution predictions of both models. They are 16 times spatially downsampled with respect to the input image size.

PIDNet-S [82] – cable detection. This is a member of a family of models designed for semantic segmentation. We train it without boundary-aware loss components, thus also without D branch supervision. We did this because these components are mostly useful for multi-class semantic segmentation with multiple, potentially confusing, object boundaries in the image. These issues do not arise for power line cables. We start from the ImageNet-pretrained checkpoint of the PIDNet-S model and add at the end of it a single

2×2 strided convolution layer to match the down-sampling factor of our models. We also replaced the SGD optimizer with Adam [83] and did not use the poly learning rate strategy.

RT-DETR [27] – pylon detection. This object detector uses the ResNet18 backbone [84]. As PIDNet-S, it has been designed with real-time applications in mind. It builds on top of transformer-based object detectors. We additionally combine it with SAHI [73], training and inference strategy for object detection in high-resolution images. We evaluate two variants of patched input scales. In both cases, we run the object detector over full-resolution image and its split into 1024×1024 overlapping patches, appropriately resizing the inputs for the detector and combining all of its outputs. In the second variant we additionally use similarly generated sets of 512×512 and 256×256 patches and add their detection results to the output. For evaluation, we rescale the final predicted bounding boxes to the downsampled output resolution of our model, use them to generate binary segmentation masks and convert them into distance masks. Also, for this model we initialize it with the pretrained weights provided with the official model implementation, obtained from training on the Objects365 [85] dataset and subsequent fine-tuning on the COCO [86] dataset.

PIDNet-S [82] – joint cables and pylons detection. We added additional segmentation heads to three branches of the PIDNet-S model to enable joint prediction of cables and pylons segmentation masks, as in our own model. In the loss function, we duplicate the cross-entropy term for the newly added pylon branch and add a weighting hyper parameter by which the added pylon segmentation loss components are multiplied. As before, we do not use boundary-aware loss components, start from the pre-trained model and use the Adam optimizer without learning rate scheduler. To match the down-sampling factor of our models the final segmentation outputs for cables and pylons are bilinearly downsampled before being passed to the loss function.

4.3 Evaluation Metrics

To compare the different models, we computed pixel-wise precision, recall and F_1 score for the generated cable and pylon segmentation masks. To

obtain these masks for our models from the predicted distance masks we simply threshold them at a selected distance value.

We also report correctness, completeness and quality (CCQ) metrics [87]. These metrics were originally applied to road extraction task and defined in terms of *lengths* of the extracted and ground-truth road segments. We implement them with respect to the *areas* of foreground objects, measured in the output resolution on the binary segmentations obtained from thresholded distance masks. Correctness and completeness operate as standard precision and recall, respectively, but include a controllable tolerance for small detection errors within the defined error margin. Those inaccuracies can stem from, for instance, imprecisions in localizing the object by the detection network or the $\mathcal{L}_{\text{MALIS}}$ loss component in cable detections, which can cause them by forcing mergers in predictions of disconnected cable line segments. In our experiments we set the tolerated error distance to a value corresponding to the closest 8-pixel neighborhood of the ground-truth segmentation foreground. In other words, the correctness and completeness should be considered as relaxed precision and recall, respectively. This relaxation can be implemented with dilation by 1 pixel of ground truth area for considering true positive detections, decreasing accordingly the area in which the detections are treated as false positives and counting as a false negative any exact ground-truth pixel which is not covered by 1-pixel-dilated exact prediction. Effectively, these metrics are insensitive to the spurious or lacking detections in the predicted segmentation masks if those are found within the tolerated error distance from the exact ground-truth.

We did not use a held out test set for either of the datasets. Instead, in the development of our model we mostly relied on a fixed train/validation split of the DDLN dataset, as well as on a 5-fold cross validation split. For the performance comparisons presented below, we report the validation performance obtained from running a single 5-fold cross validation for each model. Since both datasets contain temporally dependent image sequences, we partitioned the data into folds by splitting on the recordings level. Additionally, for the 5-fold cross validation we grouped the recordings so as to minimize the overlap of the same geographical locations within single folds.

The reported metrics are for the model states at epochs at which the mean validation quality of the target object segmentation was the highest during each respective 5-fold cross validation run. The target objects are cables or pylons, depending on the specific performance comparison presented in the tables below. For models performing joint cables and pylons segmentation, the cables are selected as target objects and pylon detection metrics are reported as achieved at the respective epochs. We report the means and standard deviations of each metric computed across all validation folds.

4.4 Performance Evaluation

Cable Only Detection.

Table 1 shows the main performance comparison between the two variants of our model and for the DeepWireCNN [1], both on the NE-VBW dataset and our DDLN dataset. We also measured inference speed as a number of processed $1 \times 3 \times 4096 \times 3000$ random input tensors per second (i.e. frames per second, FPS) on a NVidia V100 GPU. Additionally, Figure 4 depicts qualitative results. After tuning the hyperparameters of the DeepWireCNN model we achieved 0.70 ± 0.09 AP for the segmentation of cables at coarse resolution and the values for the remaining metrics as reported in the first row of the Table 1. The results on NE-VBW dataset demonstrate that both the small and the large variant of our model outperform DeepWireCNN on all cable detection metrics. Additionally, they do so without increasing the inference time. We also observed that our models achieve high performance scores earlier in the learning process than the DeepWireCNN. We attribute this to the initialization of the networks with the pretrained weights. Focusing only on our models, it is also clear that the larger variant achieves better or equivalent performance to its smaller counterpart across all cable detection metrics.

In Table 2 we compare the cable detection performance of our DDLN-M model against that of PIDNet-S [82]. As the latter is designed for real-time performance, we also report the model size and inference speeds for the networks. The size is given as the number of millions of trainable parameters in the respective model. Regarding detection performance, our DDLN-M model,

which has the same size as PIDNet-S, yields slightly better cable detection quality and a similar F_1 score. Given this result, we conducted additional experiments with PIDNet-S trained to simultaneously detect cables and pylons, as previously described in section 4.2, and compared its performance on both tasks with our joint detection model, which we detail below.

Joint Cable and Pylon Detection.

To continue the comparison of our method with the PIDNet-S [82] baseline, we added to the latter a second segmentation output head to enable it to also perform pylon detection. We report our results in Table 3 and shown in Figure 6 the evolution of the validation score during training. Our DDLN-M model still outperforms PIDNet-S on the cable detection quality, as well as on the previously equal F_1 score. It also delivers minimally higher pylon detection quality, while it records a slightly lower F_1 score than PIDNet-S. Identical observations can be made by looking at the Figure 6 where validation performance curves of our DDLN-M model are consistently, and across all validated epochs, above those of PIDNet-S for cable detection quality and F_1 score. As in the metrics reported in Table 3, pylon detection quality of DDLN-M is also minimally above that of PIDNet-S, while pylon detection F_1 score is slightly below the one of the segmentation baseline. Furthermore, recall from Table 1 that DDLN-L performs even better.

Regarding the network inference speeds, PIDNet-S is the faster one with 22.2 FPS compared to our 10.7. However, this high speed provided by PIDNet-S may not be absolutely necessary for a possible deployment of our method. We have successfully integrated DDLN-S, the less performant but faster smaller alternative of our model, in a hardware system operating in real-time onboard of a helicopter. We run the system in flight and reached 5 FPS inference speed. This is already a good running speed for the application purpose of an aircraft safety system.

Additional results for our models trained jointly for cables and pylons detection on the DDLN dataset are shown at the bottom of Table 1. Qualitative results are shown in Figure 5. The cable detection performance metric is not significantly affected by adding joint detection of pylons. It can be hypothesized that the model trained

Table 1: Comparison of power line cables detection performance between our method and DeepWireCNN (DWCNN) [1] on the NE-VBW and DDLN datasets. Results for the two size variants of our models are shown – DDLN-S and DDLN-L. DDLN-S has 2.7 million trainable parameters, about the same amount as the DeepWireCNN model.

Method	Object	FPS	Precision	Recall	F ₁	Correctness	Completeness	Quality
NE-VBW								
DWCNN	cables	9.2	0.71 ± 0.07	0.63 ± 0.06	0.66 ± 0.06	0.73 ± 0.07	0.72 ± 0.07	0.57 ± 0.08
DDLN-S	cables	12.8	0.74 ± 0.09	0.70 ± 0.08	0.71 ± 0.04	0.79 ± 0.06	0.79 ± 0.07	0.65 ± 0.05
DDLN-L	cables	9.1	0.73 ± 0.07	0.83 ± 0.06	0.78 ± 0.06	0.79 ± 0.07	0.90 ± 0.05	0.72 ± 0.07
DDLN (cables)								
DWCNN	cables	9.2	0.52 ± 0.09	0.42 ± 0.06	0.47 ± 0.07	0.54 ± 0.09	0.49 ± 0.06	0.35 ± 0.07
DDLN-S	cables	12.8	0.56 ± 0.12	0.64 ± 0.04	0.59 ± 0.09	0.65 ± 0.14	0.74 ± 0.03	0.53 ± 0.10
DDLN-L	cables	9.1	0.71 ± 0.06	0.73 ± 0.05	0.72 ± 0.05	0.83 ± 0.05	0.80 ± 0.04	0.69 ± 0.06
DDLN (cables and pylons)								
DDLN-S (joint)	cables	12.8	0.59 ± 0.08	0.60 ± 0.05	0.59 ± 0.06	0.67 ± 0.08	0.70 ± 0.05	0.52 ± 0.07
	pylons		0.41 ± 0.08	0.40 ± 0.07	0.39 ± 0.04	0.68 ± 0.07	0.56 ± 0.10	0.43 ± 0.06
DDLN-L (joint)	cables	9.1	0.71 ± 0.05	0.75 ± 0.05	0.73 ± 0.04	0.83 ± 0.04	0.82 ± 0.04	0.70 ± 0.04
	pylons		0.41 ± 0.10	0.61 ± 0.04	0.48 ± 0.08	0.71 ± 0.11	0.76 ± 0.03	0.58 ± 0.07

Bolded results highlight the best mean metric value within each group of the given dataset and the detected object type.

Table 2: Comparison of cable detection performance on DDLN dataset between our models and PIDNet-S [82], a modern semantic segmentation network for real-time applications. PIDNet-S was trained for cable detection only, while our models were trained jointly for cables and poles detection.

Method	Size	FPS	Precision	Recall	F ₁	Corr.	Compl.	Quality
PIDNet-S	7.6	22.2	0.74 ± 0.07	0.69 ± 0.05	0.71 ± 0.06	0.81 ± 0.07	0.76 ± 0.04	0.65 ± 0.07
DDLN-M	7.5	10.7	0.71 ± 0.07	0.71 ± 0.05	0.71 ± 0.06	0.83 ± 0.06	0.80 ± 0.04	0.68 ± 0.06

for cable detection alone has already implicitly learned to rely on pylon presence contextual cues. Alternatively, the models trained for the joint prediction leverage the supervision for the pylon detection task to adapt their cable detection outputs, but affecting the detection of power lines both positively and negatively, with both contributions equalizing in the final scores. However, as for independent cable detection, pylon detection performance also improves with increased model size.

In other words, relying on pylon detections for cable detection, which the network may learn to do in joint prediction setting, can be a double-edged sword. Power line cable presence does not have to be accompanied by a visible presence of pylon structures. Multiple occlusion scenarios can occur when the pylons exist but are hidden behind terrain, buildings etc. or are outside of the current field of view. Furthermore, for cables close to the camera, the associated pylons, even if contained within the camera frustum, may fall out of the

receptive field of the network for the given cable section. Moreover, the power line cables can also be attached to other structures, e.g. mounted on the rooftops of the buildings. Finally, the cables or other wiry objects which also pose the danger to the low-altitude aircraft do not have to be transmission lines *per se*. As such they are not related to the presence of transmission towers. Therefore, in some scenarios pylon detection may be helpful in finding poorly visible cables by inferring their presence from the better visible pylons to which these cables are most likely attached. In other situations, the model could rely too heavily on pylon detections to determine whether the power line cable exists at a certain location and fail to detect it independently.

Pylon Only Detection.

Finally, we compare our models against RT-DETR [27] in table 4 focusing on the pylon detection alone. In the presented results we adapt two kinds of thresholds used to turn RT-DETR predictions into distance masks: a cutoff confidence

Table 3: Comparison of joint cables and pylons detection performance on DDLN dataset between DDLN-M and PIDNet-S [82]. PIDNet-S was trained for cable and pylon detection jointly as described in section 4.2. The reported metrics are measured at the epochs with the highest validation cable detection quality.

Method	Object	Precision	Recall	F ₁	Corr.	Compl.	Quality
PIDNet-S	cables	0.70 ± 0.05	0.68 ± 0.04	0.69 ± 0.04	0.81 ± 0.03	0.76 ± 0.04	0.65 ± 0.05
	pylons	0.55 ± 0.04	0.59 ± 0.02	0.57 ± 0.03	0.71 ± 0.04	0.68 ± 0.02	0.53 ± 0.03
DDLN-M	cables	0.73 ± 0.06	0.70 ± 0.06	0.71 ± 0.05	0.86 ± 0.06	0.78 ± 0.05	0.69 ± 0.07
	pylons	0.52 ± 0.11	0.56 ± 0.04	0.53 ± 0.06	0.74 ± 0.10	0.66 ± 0.04	0.54 ± 0.05

threshold filtering out the least certain bounding box predictions and a distance mask threshold used to convert a distance mask, derived from predicted bounding boxes, into a segmentation mask. The choice of these hyperparameters is different depending on whether we optimize for best quality or F₁ score, therefore we report both, underlining the metric with respect to which we optimized the thresholds.

Firstly, looking at the two variants of inference done with the RT-DETR object detector we find that using either multiple scales of overlapping input image patches (with sizes of 256 × 256 px, 512 × 512 px and 1024 × 1024 px) or just a single scale (1024 × 1024 px patches) does not change the obtained final performance much, with single scale providing with slightly higher performance. Using multiple scales affects greatly the inference speed of the model, as each level of smaller patch size adds roughly four times more input images to process per frame than found on the previous patch size level.

Comparing RT-DETR with our approach, we note that if we grow the size of our model to nearly match the size of this object detector, our network outperforms it on correctness, completeness, quality and recall metrics and falls short on segmentation precision and F₁ score. Focusing on the precision, we can observe though that its relaxed version—correctness—is much larger than its exact version for our models. That indicates that a large part of the pylon pixels predicted by our DDLN-H model and treated as false positives is actually away from the pylon segmentation ground-truth only by the distance smaller or equal to the error margin, as previously described in section 4.3.

One reason for our superior performance on the CCQ metrics is due to the fact that those

give, by design, more favourable evaluation to the method inherently using distance mask regression than to the one in which the distance masks are only derived from a different representation – precisely regressed bounding boxes, as done for RT-DETR. The distance mask regression objective imposes a distance-dependent structure on the outputs regressed by our networks. This structure is also maintained when a segmentation mask is obtained through distance mask thresholding. Finally, the CCQ metrics, which relax standard precision and recall, also have a distance-dependent component in their use of error tolerance margin, which interplays favourably with the imposed distance-dependent structure of our targets. Meanwhile, the distance masks generated for RT-DETR are only derived with exact Euclidean distance transform from originally predicted bounding boxes. Therefore, they do not naturally inherit the distance-dependent structure in the resulting distance mask representation of the object detector’s original output.

We hypothesize that another reason for the favourable CCQ evaluation of the distance mask approach can be found in the cases concerning distant pylons clustered into groups. Those are not individually distinguishable on the predicted distance masks and an inaccurate or incomplete segmentation of partially detected pylon groups may not affect the metrics negatively. For example, if spurious foreground detections happen to fall into the region corresponding to the less clearly detected neighboring pylon, this will not have a negative impact on the CCQ metrics.

Nonetheless, our model performs well in comparison to RT-DETR, while it is simultaneously successfully detecting cable presence, using the same distance regression based method. The joint detection of power line cables is something that an

object detector like RT-DETR is not well suited to do. The cables are extremely elongated and thin objects, found in various orientations. Detecting them with an object detector method would mean that the ground truth bounding boxes would have highly variable size, be frequently largely overlapping with each other or would need to encompass cable groups as single objects and that they would contain mostly background objects and texture within their bounds.

4.5 Implementation Details

Distance and segmentation masks. To generate learning targets for our models, we converted the annotations into distance masks by computing unsigned Euclidean distance transform to the detected objects (cables and pylons). For the DDLN, we treat as object areas 5-pixel-thick regions around annotation polylines and the insides of the pylons’ bounding boxes. The target distance regression masks are first computed in pixel distance units, then clamped to the maximum distance value of 128 and finally normalized to the $[0, 1]$ range. The distance masks are downsampled through 16×16 min-pooling operation to provide the targets for learning at the coarse resolution. To generate segmentation masks used by our baselines – DeepWireCNN [1] and PIDNet-S [82], we binarized full resolution distance masks with a distance value threshold of 32. Then we downsampled the labels to match the output resolution. To perform the downsampling n times we look at the center 4 pixels of $n \times n$ patches and if they contain a foreground object we label the pixel in the downsampled output as foreground as well, and as background otherwise.

Patch sampling. For the experiments run on NE-VBW dataset and also for those using DeepWireCNN, we followed the patch sampling procedure proposed by Stambler et al. [1]. For all other experiments, we use our own sampling method. We select patch center locations dynamically during training from the high-resolution images, based on the data annotations. Patches are sampled as centered on some part of the target detected object or within its vicinity, with a set maximal allowed distance to the closest object and ensuring that the entire patch remains within the image boundaries. This effectively implements sampling position with random horizontal and

vertical jitter. When training our cable detection and joint cable and pylon detection models we do not sample purely background patches. We did so only when training the baselines models, where this setting was one of the hyperparameters. In most experiments we centered the sampled patches on power line cables. This procedure was different when training pylon-only detection model – RT-DETR [27] – where we analogously centered the sampled patches on pylons instead of cables. It was also different when training PIDNet-S [82] and DDLN-M models for comparing the joint detection performance in table 3. In those experiments we centered patches within the union of close-to-cables and close-to-pylons areas.

Data augmentations. For the models trained on the NE-VBW dataset, we used the set of augmentations proposed in [1]. For all our models trained on the DDLN dataset, as well as for PIDNet-S [82], we use color jittering and random horizontal flipping. Since the weights of these models were initialized with those obtained by pretraining on the ImageNet [42] dataset, we normalize the input with the standard ImageNet mean and variance statistics. The RT-DETR was trained with a larger set of augmentations, including color jittering, random zoom-out, IoU crop and horizontal flipping; we refer the interested reader to the work of Zhao et al. [27] and the official implementation of this object detector where this data augmentations set can be found. All the models were trained with large image patches of 1024×1024 px size.

Hyperparameters. For all models we compare against, we tuned selected sets of their hyperparameters on one of the splits of the NE-VBW dataset or on our train/validation development split of DDLN. For this procedure we used SMAC3 [88], a framework implementing Bayesian optimization and Hyperband (BOHB) [89] for hyperparameter optimization. To obtain the reported performance metrics values we run the 5-fold cross validation with the model and data augmentations configured according to the found best performing hyperparameters configurations. Finally, when thresholding on the probabilities predicted by DeepWireCNN [1] and PIDNet-S [82]

Table 4: Comparison of pylon detection on DDLN dataset between our distance mask regression method and RT-DETR [27] combined with SAHI [73]. Our models were trained jointly for cables and pylons detection. The metrics for our models are reported for epochs with the best mean validation pylon detection quality. For RT-DETR runs, the reported epochs were selected as ones with maximal mean validation value of the underlined metric – quality or F_1 . The outputs of the models are evaluated with distance masks of 32 times smaller resolution than the input image size, corresponding to the size of the output of the DDLN-H model.

Method	Size	FPS	Precision	Recall	F_1	Corr.	Compl.	Quality
RT-DETR	20.1	0.9	0.62 ± 0.12	0.50 ± 0.09	<u>0.55 ± 0.09</u>	0.71 ± 0.14	0.58 ± 0.12	0.47 ± 0.12
			0.25 ± 0.05	0.50 ± 0.09	<u>0.33 ± 0.07</u>	0.74 ± 0.10	0.75 ± 0.05	<u>0.60 ± 0.05</u>
RT-DETR ^s	20.1	16.5	0.64 ± 0.06	0.50 ± 0.09	<u>0.56 ± 0.08</u>	0.74 ± 0.09	0.58 ± 0.06	0.49 ± 0.06
			0.26 ± 0.05	0.52 ± 0.08	<u>0.34 ± 0.06</u>	0.75 ± 0.07	0.76 ± 0.05	<u>0.61 ± 0.05</u>
DDLN-H	18.3	8.8	0.45 ± 0.07	0.61 ± 0.03	0.51 ± 0.05	0.83 ± 0.04	0.79 ± 0.04	0.68 ± 0.03

^s – single scale of input image patches (1024×1024).

models, as well as on confidence scores and on distance masks derived from RT-DETR [27] predictions, we also choose threshold values which maximize the validation metrics of the obtained target object segmentation. We choose these threshold values for each data fold separately, maximizing their respective validation performance, therefore the reported mean metrics represent the best achievable performance, providing very strong baseline results for our models to compare with.

For our cable detection models, we selected the hyper parameters firstly mostly manually, throughout the method development process, and then by trying out several configurations and running with them the complete 5-fold cross validation experiments. Finally, we selected the configurations achieving the best maximal mean validation cable or pylon segmentation quality. We also selected thresholds, same for all folds in a single 5-fold cross validation run, for converting predicted distance masks into segmentations so as to maximize the detection validation quality metric, both for cables and pylons. We resorted to some automated tuning with SMAC3 [88] for our comparison with PIDNet-S [82] for joint cables and pylons detection.

We note that selection of these hyperparameters is important for the final performance. In the process we found that with improperly selected values, the DDLN-S model achieved on the NE-VBW dataset the performance equivalent to that of DeepWireCNN model.

4.6 Ablations

To demonstrate the impact of the components used in the proposed method on the performance of power line cable detection, we run ablation experiments with the DDLN-S model trained on the NE-VBW dataset for independent cable detection. Their results are presented in the table 5.

Initializing the model with pretrained weights and training it with simple MSD loss provides a highly precise model – with high precision and correctness scores. However, the same model has low recall and completeness, missing a lot of cable detections, which in turn negatively affects the quality metric. We note however, that the initialization of our ConvNeXt-Tiny backbone with pre-trained weights is indispensable to allow for successful training of our model – we did not succeed in training this model in the same manner but from scratch.

The results are similarly improved by either adding the inverse frequency based weight terms, as in \mathcal{L}_{dat} from equation (2), or by adding just $\mathcal{L}_{\text{MALIS}}$, the loss term promoting cable detections connectivity, to the plain MSD loss. Thanks to these additions the recall and the completeness increase significantly compared to the model trained only with the simple MSD loss.

For our complete setup we used both the \mathcal{L}_{dat} and $\mathcal{L}_{\text{MALIS}}$, which is the configuration for the model presented in all result tables apart from table 5. However, comparing the evolution of the validation cable segmentation quality metric during training for the complete setup and for those using either of the loss function components in isolation, it is apparent that these configurations are

Table 5: Ablation study demonstrating the impact of the components in our proposed method on cable detection performance. The ablation experiments have been conducted with the DDLN-S model on the NE-VBW [1] dataset. “Pretr.” indicates the initializing the model parameters with the weights of ConvNeXt-Tiny pretrained on the ImageNet [42] dataset. “LIF” refers to logarithmically scaled inverse frequency weights in \mathcal{L}_{dat} . $\mathcal{L}_{\text{MALIS}}$ [50] refers to the loss term promoting connectivity in cable detections.

Pretr.	LIF	$\mathcal{L}_{\text{MALIS}}$	Precision	Recall	F ₁	Correctness	Completeness	Quality
✓	–	–	0.85 ± 0.08	0.49 ± 0.17	0.60 ± 0.14	0.88 ± 0.06	0.56 ± 0.19	0.51 ± 0.16
✓	✓	–	0.75 ± 0.11	0.67 ± 0.08	0.70 ± 0.04	0.78 ± 0.09	0.75 ± 0.09	0.61 ± 0.05
✓	–	✓	0.67 ± 0.15	0.71 ± 0.09	0.67 ± 0.07	0.74 ± 0.13	0.81 ± 0.09	0.62 ± 0.08
✓	✓	✓	0.74 ± 0.09	0.70 ± 0.08	0.71 ± 0.04	0.79 ± 0.06	0.79 ± 0.07	0.65 ± 0.05

actually leading to equal performance for cable-only detection. We also note that the final scores depend here on the value of the used binarization threshold with which we convert distance masks into segmentation masks. In our experiments we observed that with a lower threshold value, using solely $\mathcal{L}_{\text{MALIS}}$ component gives better cable segmentation quality than \mathcal{L}_{dat} alone or both loss components jointly. However, overall the performance was lower than in the ablation experiments presented here in which we used a larger binarization threshold. Ultimately, for all the runs of our models reported in the previously described result tables we used both loss components and the larger binarization threshold value.

5 Conclusion

We have proposed a vision-based approach to joint detection of power line cables and transmission towers as seen by low-flying aircrafts. To this end, we have combined a modern convolutional architecture with transfer learning and a loss function adapted to curvilinear structure delineation [50]. We use a single network for both detection tasks and demonstrated its performance on two benchmarking datasets.

As all methods, ours suffer from some limitations, some inherent to the general vision-based detection methodology and others that can be remedied by further work. Firstly, our method yields localized detections of power line cables and pylons in the form of segmentation masks. For training, we rely on bounding box annotations of the pylons, which are not particularly accurate representations for the not distant ones. More precise segmentation masks could be used instead in

situations where the pylons’ structure and background can be easily separated. Another avenue worth pursuing is to study how much the model relies on pylon predictions for cable detections, and *vice versa*, as discussed in section 4.4. This aspect is important when deploying our approach in unusual scenarios that may not exhibit the same correlations as our training set. Also vertical obstacles that can be confused for pylons should be studied separately. Finally, the appearance of power line cables and pylons naturally varies under weather and lighting conditions, and also between different geographical locations with differing power lines infrastructure. Any vision-based deep learning method, such as ours, relies on a model trained on an ultimately limited dataset and therefore with a limited set of appearances for the obstacles that it is capable of handling.

Increasing the inference speed of our model should also constitute a direction for future work. To achieve it, modifications in architectural components of the model backbone should be considered, a single example of which can be found in InceptionNeXt [90] regarding depth-wise convolutions. Incorporating attentional components into the model architecture, as can be found in PID-Net [82], also presents a viable research direction, with the aim of increasing the receptive field and the expressivity of the network.

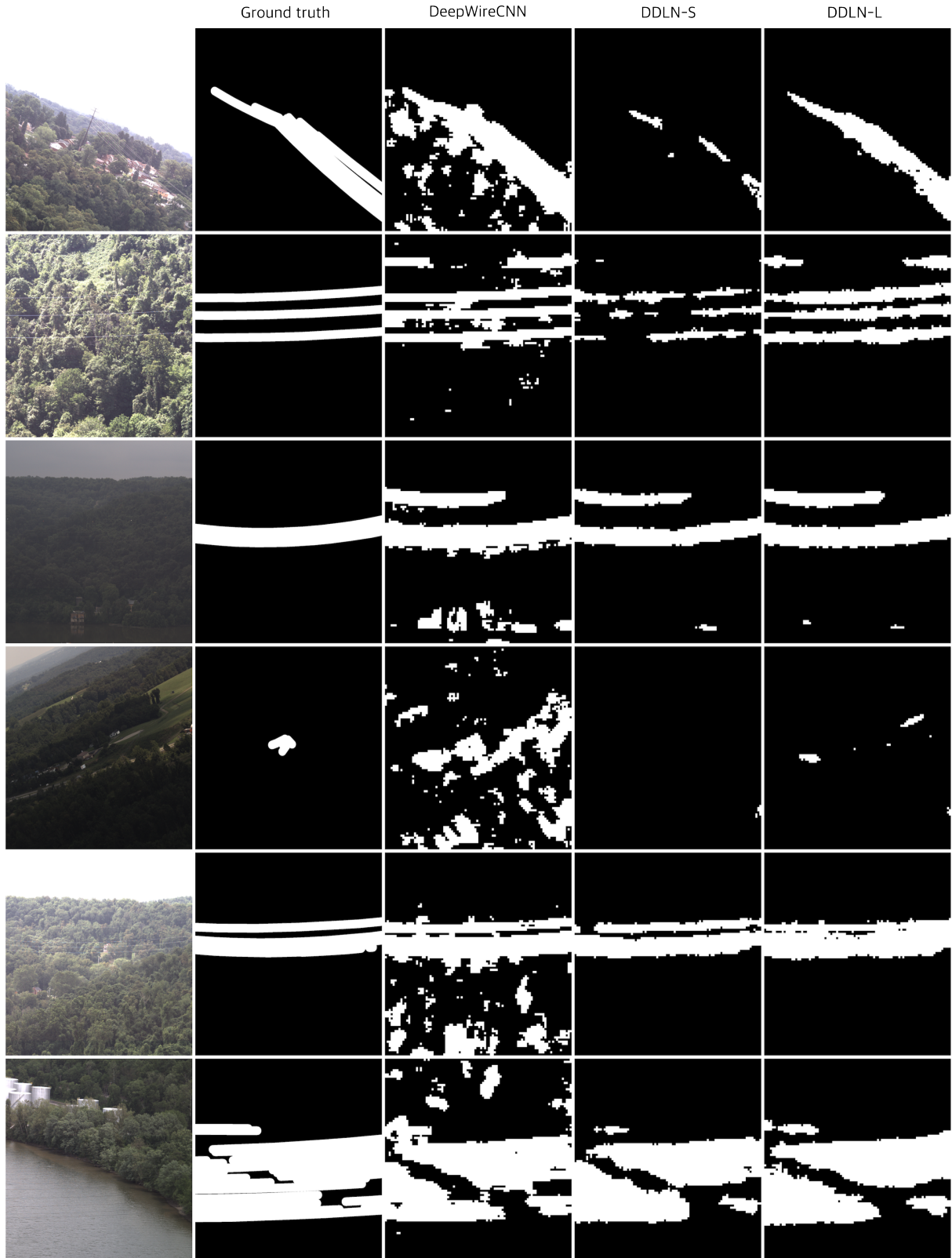


Fig. 4: Exemplary predictions of the three models trained on the NE-VBW dataset [1]: DeepWireCNN [1], DDLN-S and DDLN-L. The inputs are 1536×1536 px crops from full-resolution images from the validation set. Predictions were generated by models initialized from checkpoints at epochs with highest validation cable segmentation quality metric.

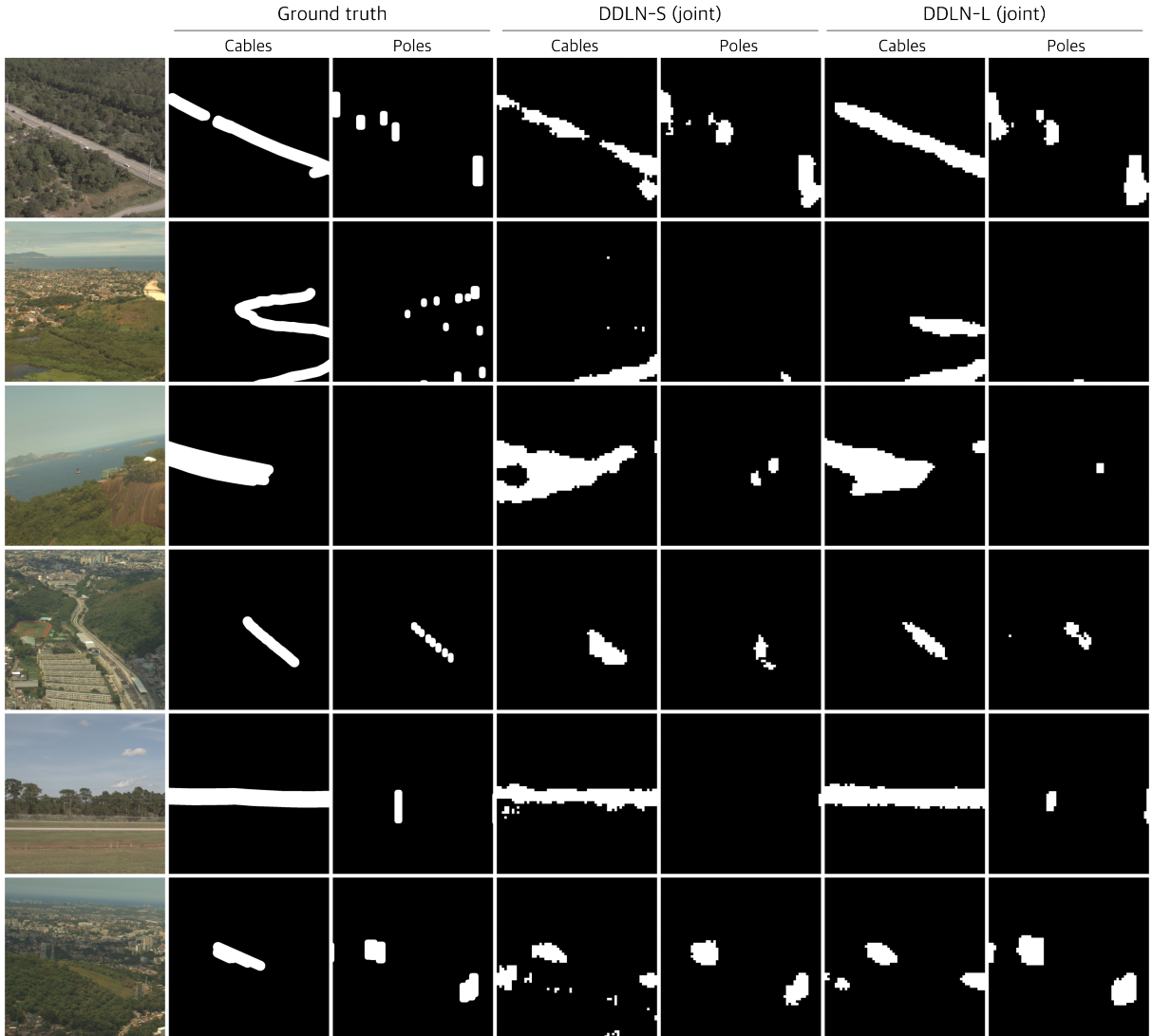


Fig. 5: Exemplary predictions of the two size variants of our model trained jointly for cable and pylon detection on the DDLN dataset. The inputs are 1024×1024 px crops from full-resolution images from the validation set. Predictions were generated by models initialized from checkpoints at epochs with highest validation cable segmentation quality metric.

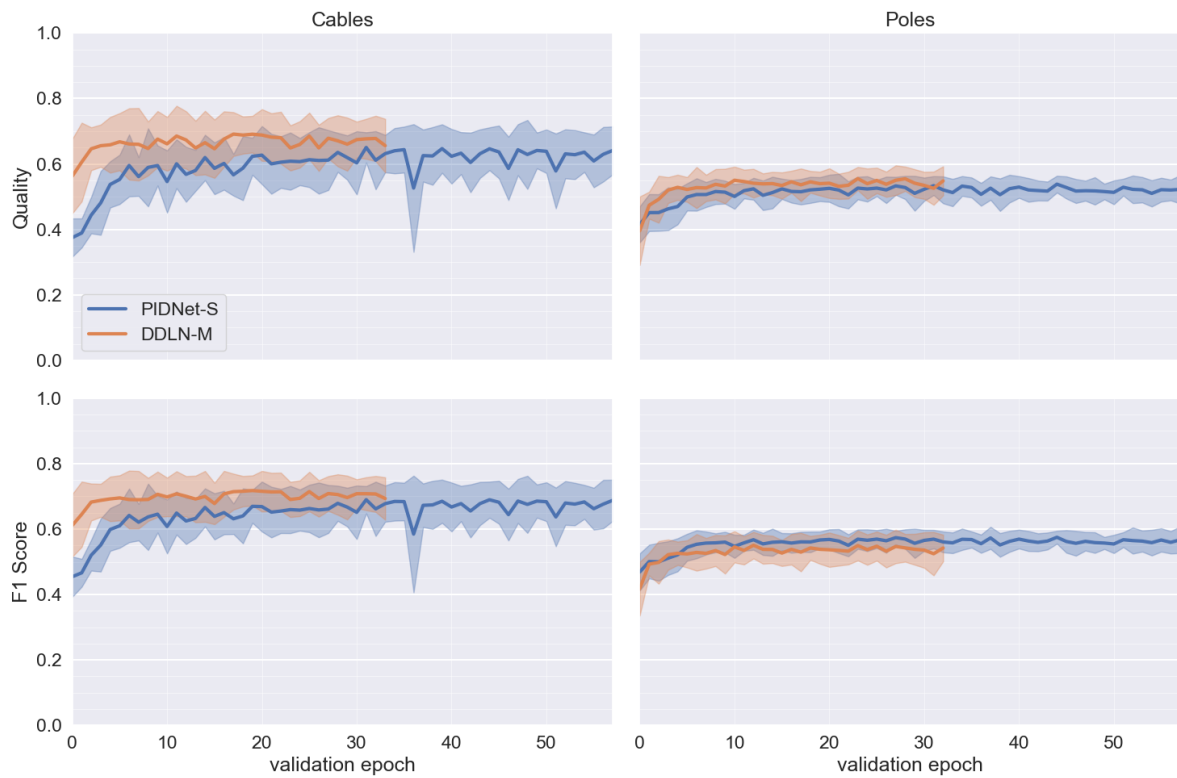


Fig. 6: Evolution of validation metrics – quality and F_1 for cable and pylon detection – in 5-fold cross validation runs reported in table 3 for DDLN-M and PIDNet-S [82], both trained for joint detection task. The solid lines are means of respective metrics, while the shaded areas correspond to standard deviations.

References

- [1] Stambler, A., Sherwin, G., Rowe, P.: Detection and Reconstruction of Wires Using Cameras for Aircraft Safety Systems. In: International Conference on Robotics and Automation (2019)
- [2] Miller, E.: Flying in the Wire Environment. Safety alert for operators, U. S. Department of Transportation, Federal Aviation Administration (2010)
- [3] Flanigen, P.: Algorithms and Visualizations to Support Airborne Detection of Vertical Obstacles. PhD thesis, University of Michigan (2023)
- [4] FLARM Technology: Traffic and Collision Warning. <https://www.flarm.com/>
- [5] Campoy, P., Garcia, P.J., Barrientos, A., Cerro, J.D., Aguirre, I., Roa, A., Garcia, R., Muñoz, J.M.: An Stereoscopic Vision System Guiding an Autonomous Helicopter for Overhead Power Cable Inspection. In: Robot Vision: International Workshop RobVis 2001 Auckland, New Zealand, February 16–18, 2001 Proceedings, pp. 115–124 (2001)
- [6] Rangachar, K., Camps, O.I.: Wire Detection Algorithms for Navigation. Technical report, NASA (2002)
- [7] Yan, P., Khan, S.M., Shah, M.: 3D Model Based Object Class Detection in an Arbitrary View. In: International Conference on Computer Vision (2007)
- [8] Candamo, J., Kasturi, R., Goldgof, D., Sarkar, S.: Detection of Thin Lines Using Low-Quality Video from Low-Altitude Aircraft in Urban Settings. IEEE Transactions on Aerospace and Electronic Systems (2009)
- [9] Tilawat, J., Theera-Umpon, N., Auephanwiriyaikul, S.: Automatic Detection of Electricity Pylons in Aerial Video Sequences. In: 2010 International Conference on Electronics and Information Engineering (2010)
- [10] Sampedro, C., Martinez, C., Chauhan, A., Campoy, P.: A Supervised Approach to Electric Tower Detection and Classification for Power Line Inspection. In: International Joint Conference on Neural Networks (IJCNN) (2014)
- [11] Cerón, A., Mondragón, I., Prieto, F.: Real-Time Transmission Tower Detection from Video Based on a Feature Descriptor. IET Computer Vision **11**(1), 33–42 (2017)
- [12] Pan, C., Cao, X., Wu, D.: Power Line Detection via Background Noise Removal. In: GlobalSIP (2016)
- [13] Gubbi, J., Varghese, A., Balamuralidhar, P.: A New Deep Learning Architecture for Detection of Long Linear Infrastructure. In: Machine Vision and Applications (2017)
- [14] Lee, S.J., Yun, J., Choi, H., Kwon, W., Koo, G., Kim, S.W.: Weakly Supervised Learning with Convolutional Neural Networks for Power Line Localization. In: Symposium Series on Computational Intelligence (2017)
- [15] Li, Y., Pan, C., Cao, X., Wu, D.: Power Line Detection by Pyramidal Patch Classification. IEEE Transactions on Emerging Topics in Computational Intelligence **3**(6), 416–426 (2018)
- [16] Madaan, R., Maturana, D., Scherer, S.: Wire Detection Using Synthetic Data and Dilated Convolutional Networks for Unmanned Aerial Vehicles. In: International Conference on Intelligent Robots and Systems, pp. 3487–3494 (2017)
- [17] Bian, J., Hui, X., Zhao, X., Tan, M.: A Novel Monocular-Based Navigation Approach for UAV Autonomous Transmission-Line Inspection. In: International Conference on Intelligent Robots and Systems, pp. 1–7 (2018)
- [18] Zhu, G., Zhang, W., Wang, M., Wang, J., Fang, X.: Corner guided instance segmentation network for power lines and transmission towers detection. Expert Systems with Applications **234** (2023)
- [19] Liu, Z., Mao, H., Wu, C., Feichtenhofer,

- C., Darrell, T., Xie, S.: A Convnet for the 2020s. In: Conference on Computer Vision and Pattern Recognition (2022)
- [20] Yetgin, Ö.E., Gerek, Ö.N.: Automatic Recognition of Scenes with Power Line Wires in Real Life Aerial Images Using Dct-Based Features. *Digital Signal Processing* **77**, 102–119 (2018)
- [21] Yetgin, Ö.E., Benligiray, B., Gerek, Ö.N.: Power Line Recognition from Aerial Images with Deep Learning. *IEEE Transactions on Aerospace and Electronic Systems* **55**(5), 2241–2252 (2018)
- [22] Yetgin, Ö.E., Gerek, Ö.N.: Ground Truth of Powerline Dataset (Infrared-IR and Visible Light-VL) (2019). <https://doi.org/10.17632/twpx8xccsw.9>
- [23] Zhang, H., Yang, W., Yu, H., Zhang, H., Xia, G.: Detecting Power Lines in UAV Images with Convolutional Features and Structured Constraints. *Remote Sensing* (2019)
- [24] Abdelfattah, R., Wang, X., Wang, S.: TTPLA: An Aerial-Image Dataset for Detection and Segmentation of Transmission Towers and Power Lines. In: Asian Conference on Computer Vision. Springer, ??? (2021)
- [25] Choi, H., Yun, J.P., Kim, B.J., Jang, H., Kim, S.W.: Attention-Based Multimodal Image Feature Fusion Module for Transmission Line Detection. *IEEE Transactions on Industrial Informatics* **18**(11), 7686–7695 (2022)
- [26] Chiu, M.T., Zhang, X., Wei, Z., Zhou, Y., Shechtman, E., Barnes, C., Lin, Z., Kainz, F., Amirghodsi, S., Shi, H.: Automatic High Resolution Wire Segmentation and Removal. In: Conference on Computer Vision and Pattern Recognition, pp. 2183–2192 (2023)
- [27] Zhao, Y., Lv, W., Xu, S., Wei, J., Wang, G., Dang, Q., Liu, Y., Chen, J.: DETRs beat YOLOs on Real-time Object Detection. In: Conference on Computer Vision and Pattern Recognition (2024)
- [28] Song, S., Xiao, J.: Sliding Shapes for 3D Object Detection in Depth Images. In: European Conference on Computer Vision (2014)
- [29] Tian, F., Wang, Y., Zhu, L.: Power Line Recognition and Tracking Method for UAVs Inspection. In: IEEE International Conference on Information and Automation (2015)
- [30] Baker, L., Mills, S., Langlotz, T., Rathbone, C.: Power Line Detection Using Hough Transform and Line Tracing Techniques. In: International Conference on Image and Vision Computing New Zealand (IVCNZ) (2016)
- [31] Santos, T., Moreira, M., Almeida, J., Dias, A., Martins, A., Dinis, J., Formiga, J., Silva, E.: Plined: Vision-Based Power Lines Detection for Unmanned Aerial Vehicles. In: IEEE International Conference on Autonomous Robot Systems and Competitions, pp. 253–259 (2017)
- [32] Oh, J., Lee, C.: 3D Power Line Extraction from Multiple Aerial Images. *Sensors* (2017)
- [33] Ganovelli, F., Malomo, L., Scopigno, R.: Reconstructing Power Lines from Images. *Image and Vision Computing New Zealand* (2018)
- [34] Zhou, Z., Liu, X., Long, B., Peng, H.: TRemap: Automatic 3D Neuron Reconstruction Based on Tracing, Reverse Mapping and Assembling of 2D Projections. *Neuroinformatics* **14**(1), 41–50 (2016)
- [35] Nguyen, V.H., Jenssen, R., Roverso, D.: LsNet: Fast Single-Shot Line-Segment Detector. *Machine Vision and Applications* (2020)
- [36] Bolya, D., Zhou, C., Xiao, F., Lee, Y.J.: Yolact: Real-Time Instance Segmentation. In: International Conference on Computer Vision, pp. 9157–9166 (2019)
- [37] Xing, J., Cioffi, G., Hidalgo-Carrió, J., Scaramuzza, D.: Autonomous Power Line Inspection with Drones via Perception-Aware MPC. In: International Conference on Intelligent Robots and Systems (2023)
- [38] Redmon, J., Divvala, S., Girshick, R.,

- Farhadi, A.: You Only Look Once: Unified, Real-Time Object Detection. In: Conference on Computer Vision and Pattern Recognition (2016)
- [39] Dai, Z., Yi, J., Zhang, Y., Zhou, B., He, L.: Fast and accurate cable detection using CNN. *Applied Intelligence* **50**, 4688–4707 (2020)
- [40] Simonyan, K., Zisserman, A.: Very Deep Convolutional Networks for Large-Scale Image Recognition. In: International Conference on Learning Representations (2015)
- [41] Liu, Y., Cheng, M.-M., Hu, X., Wang, K., Bai, X.: Richer Convolutional Features for Edge Detection. In: Conference on Computer Vision and Pattern Recognition, pp. 3000–3009 (2017)
- [42] Deng, J., Dong, W., Socher, R., Li, L.-J., Li, K., Fei-Fei, L.: Imagenet: A Large-Scale Hierarchical Image Database. In: Conference on Computer Vision and Pattern Recognition (2009)
- [43] Jaffari, R., Hashmani, M.A., Reyes-Aldasoro, C.C.: A Novel Focal Phi Loss for Power Line Segmentation with Auxiliary Classifier U-Net. *Sensors* **21**(8), 2803 (2021)
- [44] Cheng, Y., Chen, Z., Liu, D.: PL-UNeXt: Per-Stage Edge Detail and Line Feature Guided Segmentation for Power Line Detection. In: International Conference on Image Processing, pp. 261–265 (2023)
- [45] Abdelfattah, R., Wang, X., Wang, S.: PLGAN: Generative Adversarial Networks for Power-Line Segmentation in Aerial Images. *IEEE Transactions on Image Processing* (2023)
- [46] An, D., Zhang, Q., Chao, J., Li, T., Qiao, F., Bian, Z., Deng, Y.: Duformer: Solving Power Line Detection Task in Aerial Images Using Semantic Segmentation. In: Chinese Conference on Pattern Recognition and Computer Vision (PRCV), pp. 54–66 (2023)
- [47] Meyer, M., Galdran, A., Mendonça, A., Campilho, A.: A Pixel-Wise Distance Regression Approach for Joint Retinal Optical Disc and Fovea Detection. (2018)
- [48] Davari, A., Baller, C., Seehaus, T., Braun, M., Maier, A., Christlein, V.: Pixelwise Distance Regression for Glacier Calving Front Detection and Segmentation. *IEEE Transactions on Geoscience and Remote Sensing* (2022)
- [49] Xue, N., Wu, T., Bai, S., Wang, F., Xia, G., Zhang, L., Torr, P.S.: Holistically-Attracted Wireframe Parsing: from Supervised to Self-Supervised Learning. *IEEE Transactions on Pattern Analysis and Machine Intelligence* (2023)
- [50] Oner, D., Koziński, M., Citraro, L., Dadap, N.C., Konings, A.G., Fua, P.: Promoting Connectivity of Network-Like Structures by Enforcing Region Separation. *IEEE Transactions on Pattern Analysis and Machine Intelligence* **44**(9), 5401–5413 (2021)
- [51] Watanabe, J.: Electric Pole Detection Using Deep Network Based Object Detector. In: Remote Sensing Technologies and Applications in Urban Environments III, pp. 88–95 (2018)
- [52] Wang, H., Yang, G., Li, E., Tian, Y., Zhao, M., Liang, Z.: High-Voltage Power Transmission Tower Detection Based on Faster R-CNN and YOLO-V3. In: 2019 Chinese Control Conference (CCC), pp. 8750–8755 (2019)
- [53] Yang, Z., Chen, L., Chen, J., Lai, Z.: Object Detection and Contour Extraction of Transmission Towers Based on Computer Vision. In: Joint International Information Technology and Artificial Intelligence Conference, pp. 863–867 (2023)
- [54] Zhang, W., Witharana, C., Li, W., Zhang, C., Li, X., Parent, J.: Using Deep Learning to Identify Utility Poles with Crossarms and Estimate Their Locations from Google Street View Images. *Sensors* **18**(8), 2484 (2018)
- [55] Chen, B., Miao, X.: Distribution Line Pole Detection and Counting Based on YOLO

- Using UAV Inspection Line Video. *Journal of Electrical Engineering & Technology* **15**, 441–448 (2020)
- [56] Mo, Y., Xie, R., Pan, Q., Zhang, B.: Automatic Power Transmission Towers Detection Based on the Deep Learning Algorithm. In: 2021 2nd International Conference on Computer Engineering and Intelligent Control (ICCEIC), pp. 11–15 (2021)
- [57] Zhang, Y., Lu, X., Li, W., Yan, K., Mo, Z., Lan, Y., Wang, L.: Detection of Power Poles in Orchards Based on Improved Yolov5s Model. *Agronomy* **13**(7), 1705 (2023)
- [58] Gomes, M., Silva, J., Gonçalves, D., Zamboni, P., Perez, J., Batista, E., Ramos, A., Osco, L., Matsubara, E., Li, J., Junior, J.M., Gonçalves, W.: Mapping Utility Poles in Aerial Orthoimages Using Atss Deep Learning Method. *Sensors* **20**(21), 6070 (2020)
- [59] Haroun, F.M.E., Deros, S.N.M., Din, N.M.: Detection and Monitoring of Power Line Corridor from Satellite Imagery Using Retinanet and K-Mean Clustering. *IEEE Access* **9**, 116720–116730 (2021)
- [60] Wang, T., Wei, R., Wang, L., Zhu, L., Zhou, E., Liu, S., Yang, H., Wang, S.: Detection of Transmission Towers and Insulators in Remote Sensing Images with Deep Learning. In: 2021 China Automation Congress (CAC), pp. 3298–3303 (2021)
- [61] Zhang, Z., Xie, X., Song, C., Dai, D., Bu, L.: Transmission Tower Detection Algorithm Based on Feature-Enhanced Convolutional Network in Remote Sensing Image. In: Chinese Conference on Pattern Recognition and Computer Vision (PRCV), pp. 551–564 (2022)
- [62] Zha, W., Hu, L., Duan, C., Li, Y.: Semi-Supervised Learning-Based Satellite Remote Sensing Object Detection Method for Power Transmission Towers. *Energy Reports* **9**, 15–27 (2023)
- [63] Araar, O., Aouf, N., Dietz, J.L.V.: Power Pylon Detection and Monocular Depth Estimation from Inspection UAVs. *Industrial Robot: An International Journal* (2015)
- [64] Gioi, R.G., Jakubowicz, J., Morel, J.M., Randall, G.: LSD: A Fast Line Segment Detector with a False Detection Control. *IEEE Transactions on Pattern Analysis and Machine Intelligence* (2010)
- [65] Zhang, J., Shan, H., Cao, X., Yan, P., Li, X.: Pylon Line Spatial Correlation Assisted Transmission Line Detection. *IEEE Transactions on Aerospace and Electronic Systems* **50**(4), 2890–2905 (2014)
- [66] Lowe, D.G.: Distinctive Image Features from Scale-Invariant Keypoints. *International Journal of Computer Vision* **20**(2), 91–110 (2004)
- [67] Rosten, E., Drummond, T.: Machine Learning for High-Speed Corner Detection. In: European Conference on Computer Vision (2006)
- [68] Rublee, E., Rabaud, V., Konolidge, K., Bradski, G.: ORB: An Efficient Alternative to SIFT or SURF. In: International Conference on Computer Vision (2011)
- [69] Ren, S., He, K., Girshick, R., Sun, J.: Faster R-CNN: Towards Real-Time Object Detection with Region Proposal Networks. In: Advances in Neural Information Processing Systems (2015)
- [70] Chen, L., Yang, Z., Huang, F., Dai, Y., Liu, R., Li, J.: Transmission Tower Re-Identification Algorithm Based on Machine Vision. *Applied Sciences* **14**(2), 539 (2024)
- [71] Liu, W., Anguelov, D., Erhan, D., Szegedy, C., Reed, S.E., Fu, C.-Y., Berg, A.C.: SSD: Single Shot Multibox Detector. In: European Conference on Computer Vision (2016)
- [72] Lin, T.-Y., Goyal, P., Girshick, R., He, K., Dollár, P.: Focal Loss for Dense Object Detection. In: International Conference on Computer Vision (2017)

- [73] Akyon, F.C., Altinuc, S.O., Temizel, A.: Slicing aided hyper inference and fine-tuning for small object detection. In: International Conference on Image Processing, pp. 966–970 (2022)
- [74] Li, B., Chen, C.: Transmission Line Detection Based on a Hierarchical and Contextual Model for Aerial Images. *Journal of Electronic Imaging* **27**(4), 043054–043054 (2018)
- [75] Shan, H., Zhang, J., Cao, X., Li, X., Wu, D.: Multiple Auxiliaries Assisted Airborne Power Line Detection. *IEEE Transactions on Industrial Electronics* **64**(6), 4810–4819 (2017)
- [76] Feng, L., Zhang, L., Gao, Z., Zhou, R., Li, L.: Gabor-YOLONet: A lightweight and efficient detection network for low-voltage power lines from unmanned aerial vehicle images. *Frontiers in Energy Research* **10** (2023)
- [77] Zhencang, H., Renjie, J., Dong, L.: A Structural Information Aided Method for Intelligent Detection of Power Line Targets. In: 2023 IEEE 6th Information Technology, Networking, Electronic and Automation Control Conference (ITNEC), vol. 6, pp. 1622–1632 (2023)
- [78] Ma, W., Xiao, J., Zhu, G., Wang, J., Zhang, D., Fang, X., Miao, Q.: Transmission tower and Power line detection based on improved Solov2. *IEEE Transactions on Instrumentation and Measurement* (2024)
- [79] Redmon, J., Farhadi, A.: YOLOv3: An Incremental Improvement. In: arXiv Preprint (2018)
- [80] Turaga, S., Briggman, K., Helmstaedter, M., Denk, W., Seung, S.: Maximin Affinity Learning of Image Segmentation. In: *Advances in Neural Information Processing Systems*, pp. 1865–1873 (2009)
- [81] Funke, J., Tschopp, F.D., Grisaitis, W., *et al.*: Large Scale Image Segmentation with Structured Loss Based Deep Learning for Connectome Reconstruction. *IEEE Transactions on Pattern Analysis and Machine Intelligence* **41**(7), 1669–1680 (2018)
- [82] Xu, J., Xiong, Z., Bhattacharyya, S.P.: PID-Net: A Real-time Semantic Segmentation Network Inspired by PID Controllers. In: *Conference on Computer Vision and Pattern Recognition*, pp. 19529–19539 (2023)
- [83] Kingma, D.P., Ba, J.: Adam: A Method for Stochastic Optimization. In: arXiv Preprint (2014)
- [84] He, K., Zhang, X., Ren, S., Sun, J.: Deep Residual Learning for Image Recognition. In: *Conference on Computer Vision and Pattern Recognition*, pp. 770–778 (2016)
- [85] Shao, S., Li, Z., Zhang, T., Peng, C., Yu, G., Zhang, X., Li, J., Sun, J.: Objects365: A large-scale, high-quality dataset for object detection. In: *International Conference on Computer Vision*, pp. 8430–8439 (2019)
- [86] Lin, T.-Y., Maire, M., Belongie, S., Hays, J., Perona, P., Ramanan, D., Dollár, P., Zitnick, C.L.: Microsoft COCO: Common Objects in Context. In: *European Conference on Computer Vision*, pp. 740–755 (2014)
- [87] Wiedemann, C., Heipke, C., Mayer, H., Jamet, O.: Empirical Evaluation of Automatically Extracted Road Axes. In: *Empirical Evaluation Techniques in Computer Vision*, pp. 172–187 (1998)
- [88] Lindauer, M., Eggensperger, K., Feurer, M., Biedenkapp, A., Deng, D., Benjamins, C., Ruhkopf, T., Sass, R., Hutter, F.: SMAC3: A Versatile Bayesian Optimization Package for Hyperparameter Optimization. *Journal of Machine Learning Research* **23**(54), 1–9 (2022)
- [89] Falkner, S., Klein, A., Hutter, A.F.: BOHB: Robust and Efficient Hyperparameter Optimization at Scale. In: *International Conference on Machine Learning*, pp. 1437–1446 (2018)
- [90] Yu, W., Zhou, P., Yan, S., Wang, X.: InceptionNeXt: When Inception Meets ConvNeXt.

In: Conference on Computer Vision and Pattern Recognition, pp. 5672–5683 (2024)